RAA 2017 Vol. **17** No. **8**, 82 (12pp) doi: 10.1088/1674–4527/17/8/82

http://www.raa-journal.org *http://iopscience.iop.org/raa*

***R**esearch in*
***A**stronomy and*
***A**strophysics*

Optical multi-color monitoring of OJ 287 from 2006 to 2012

Qian Guo[1,2,3,4], Ding-Rong Xiong[1,2,3], Jin-Ming Bai[1,2,3], Xu-Liang Fan[1,2,3,4] and Wei-Min Yi[1,2,3]

[1] Yunnan Observatories, Chinese Academy of Sciences, Kunming 650216, China; *guoqian@ynao.ac.cn; baijinming@ynao.ac.cn*
[2] Key Laboratory for the Structure and Evolution of Celestial Objects, Chinese Academy of Sciences, Kunming 650216, China
[3] Center for Astronomical Mega-Science, Chinese Academy of Sciences, Beijing 100012, China
[4] University of Chinese Academy of Sciences, Beijing 100049, China

Received 2017 January 16; accepted 2017 April 30

Abstract We present our optical multi-color monitoring of the BL Lac object OJ 287 from January 2006 to December 2012 in the V, R and I bands. A relatively active state in OJ 287 has been found over all monitored epochs, among which the variations of average magnitude in $V/R/I$ bands were measured with ΔV =1.956 mag, ΔR =2.067 mag and ΔI =2.115 mag, respectively. No reliable intraday variability is detected, but possible variability is detected on 16 nights. Their relative variation amplitudes fall into the range between 1% and 8%, with the majority between 2% and 4%. No time lags have been detected, but strong correlations exist among light curves in the three wavebands. The bluer-when-brighter trend is dominant over intraday timescales, which supports the shock-in-jet model. When combining with additional V/R band data obtained from SMARTS and the Steward Observatory, we also find a bluer-when-brighter trend over a long-term timescale. Some possible periods of 513, 176, 36, 30, 26, 17 and 14 d are found in all time-series data sets from 2006 to 2017. Possible explanations about these periods are given.

Key words: BL Lacertae objects: individual (OJ 287) — galaxies: active — galaxies: photometry

1 INTRODUCTION

Blazars are an extreme subclass of active galactic nuclei, which have very rapid and strong variability over all electromagnetic wavelengths. Blazars include two subclasses, namely, BL Lacertae objects (BL Lacs) and flat-spectrum radio quasars (FSRQs). BL Lacs exhibit featureless or weak emission lines, while FSRQs have prominent emission lines in their optical spectra. The spectral energy distribution of blazars is usually characterized by a structure with two bumps. The low energy bump spanning from radio to X-ray is produced from synchrotron emission caused by relativistic jets. The radiation mechanism of the high-energy bump from X-ray to γ-ray is not quite clear, but it is most likely caused by inverse-Compton scattering (Böttcher 2007).

Variability timescales from a few minutes to years are common among blazars. Variability timescale ranging from a few minutes to hours is often defined as intraday variability (IDV) or microvariability. The timescale of short-term variability (STV) is from days to weeks or even months, while long-term variability happens from months to years (Gupta et al. 2008; Agarwal & Gupta 2015; Xiong et al. 2016). Variability timescales of blazars can provide insight on the physical processes underlying these variations, and put strong constraints on the origin of variability. Thus long-term optical monitoring is helpful for understanding the nature of blazars.

BL Lac object OJ 287 (0851+203), at a redshift of $z = 0.306$, has been observed from the late 1900s up to the present. A 12 year period had been discovered for OJ 287 by Sillanpaa et al. (1988). They proposed a binary black hole model to explain this period, and pre-

dicted that the next major outburst would take place in late 1994. Thereafter, OJ-94, an international project to monitor OJ 287 in multiple wavebands from the fall of 1993 to the beginning of 1997, confirmed the periodic outburst of OJ 287 (Wu et al. 2006; Dai et al. 2011). Besides the large long-term outburst, Wu et al. (2006) found a possible period of 40 d from their optical variability analyses. Moreover, Efimov et al. (2002) identified a 36.56 d periodic rotation of the plane of polarization in OJ 287.

In 1972, OJ 287 reached its brightest state with $V \sim 12$ mag (Qian & Tao 2003; Fan et al. 2009). The object showed an outburst in 2015 with 12.9 mag in the optical R band (Valtonen et al. 2016). Intraday variations on timescales over 10 minutes to 2 hours with magnitude variations from 0.11 mag to 0.75 mag were detected by Fan et al. (2009). Gaur et al. (2012) reported significant flux variations for STV and intraday timescales. The color behavior of OJ 287 usually shows a bluer-when-brighter trend (Takalo & Sillanpaa 1989; Carini et al. 1992; Vagnetti et al. 2003; Wu et al. 2006; Villforth et al. 2010a). However, a stable optical color index had also been found during the outburst in 1993-1994 (Sillanpaa et al. 1996). In addition, Bonning et al. (2012) found that the object showed a redder-when-brighter trend as well as a bluer-when-brighter trend.

Based on the analysis of previous observations, this object is connected with strong activities. The spectral behaviors are also complex. Therefore, we performed optical monitoring with multi-color photometry from 2006 to 2012. We analyze the variability and spectral properties of OJ 287. Combining with V band and R band data from SMARTS[1] (Bonning et al. 2012) and Steward Observatory[2] (Smith et al. 2009), we further study the spectral properties over a long-term timescale and search for possible periodic signals. The observations and data reduction procedures are described in Section 2. The results and discussions are presented in Section 3. The summary is given in Section 4.

2 OBSERVATIONS AND DATA REDUCTIONS

Our optical photometric observations of OJ 287 were carried out with the Lijiang 2.4 m and Kunming 1.02 m optical telescopes administered by Yunnan Observatories. We used the 2.4 m telescope to observe this target from 2008 to 2010, and the 1.02 m telescope from 2006 to 2012. Both telescopes are equipped with broad-band Johnson UBV and Cousins RI filters. During our observation periods, the Lijiang 2.4 m telescope was equipped with a Princeton Instruments VersArray 1300B (1340 $\times$ 1300 pixels) CCD mounted on the Cassegrain focus. The field of view was 4.48 $\times$ 4.40 arcmin^2. The readout noise and gain were 6.05 electrons/pixel and 1.1 electrons/ADU, respectively. Before 2008, the 1.02 m telescope was equipped with a 1024 $\times$ 1024 pixel CCD chip, and the field of view was 6.5 $\times$ 6.5 arcmin^2. The readout noise and gain were 3.9 electrons/pixel and 4.0 electrons/ADU, respectively. A new Andor DW436 2048 $\times$ 2048 pixel CCD camera at the Cassegrain focus has replaced the old CCD with a field of view 7.3 $\times$ 7.3 arcmin^2. The readout noise and gain are now 6.33 electrons/pixel and 2.0 electrons/ADU, respectively (Liao et al. 2014; Dai et al. 2015).

Our photometric observations were performed in V, R and I bands through two modes. The first mode was that all of the observations were completed for the same optical band and then moved to the next band. Another mode was a cyclic mode from V, R to I bands respectively. For the cyclic mode, the time resolutions were 1 - 3 minutes with the majority of time resolutions $<$ 1.5 minutes. Thus, these observations can be considered as quasi-simultaneous observations. Different exposure times were set depending on seeing and weather conditions. The bias frames were taken on each observing night. The sky flat-field images were taken in good weather conditions. Data reduction was performed by the standard IRAF routes. After correcting for the bias and flat-field, all the images were processed using the task APPHOT from the IRAF software packages. We tried different photometry apertures for every night, and then selected the aperture radii of 1.5 $\times$ FWHM for the best signal to noise ratio. The comparison stars 10 and C2 were chosen from Fiorucci & Tosti (1996) in this work. Star 10 has a similar apparent magnitude to the object and the apparent magnitude of star C2 is a little fainter than that of the object. Apparent magnitudes of the object are derived from these two comparison stars in the frame with $\frac{m_{10}+m_{C2}}{2}$ (m_{10} is the apparent magnitude obtained from comparison star 10 and m_{C2} from comparison star C2). The rms errors of the photometry on a specific night are calculated from the two comparison stars using the formula

$$\sigma = \sqrt{\frac{\sum(m_i - \overline{m})^2}{N-1}}, \quad (1)$$

[1] *http://www.astro.yale.edu/smarts/fermi*
[2] *http://james.as.arizona.edu/ psmith/Fermi/*

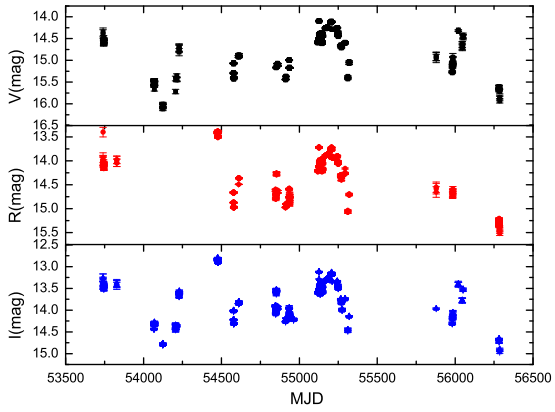

Fig. 1 The light curves from 2006 to 2012 in the V, R and I bands, from top to bottom respectively.

where $m_i = (m_{10} - m_{c2})_i$ is the differential magnitude of stars 10 and C2, while $\overline{m} = \overline{m_{10} - m_{c2}}$ is the average differential magnitude for one night, and N is the number of the observations during a given night.

For a given night, the variability amplitude (Amp) is calculated by Heidt & Wagner (1996)

$$\mathrm{Amp} = 100 \times \sqrt{(A_{\max} - A_{\min})^2 - 2\sigma^2}\ \mathrm{percent}, \quad (2)$$

where $A_{\max}$ and $A_{\min}$ are the maximum and minimum magnitudes of the blazar.

3 RESULTS AND DISCUSSION

Our optical monitoring campaign lasted seven years from January 2006 to December 2012, with 84 nights and 3805 CCD frames. The observation log is shown in Table 1. The results of observations are listed in Tables 2-4 for V, R and I bands, respectively. The light curves of our monitoring from 2006 to 2012 are presented in Figure 1. A relatively active state in OJ 287 has been found over all monitoring epochs, among which the variations of average magnitude in $V/R/I$ bands were measured with ΔV =1.956 mag, ΔR =2.067 mag and ΔI =2.115 mag, respectively.

3.1 Microvariability

For our data, we apply three different statistical tests (C-test, F-test and ANOVA-test) to quantify the IDV. Corresponding to different exposure times, we only analyze the data covering more than 9 or 15 images for each band during each night.

Table 1 An Overview of Observation Logs of OJ 287

Year (1)	Nights (2)	N (V) (3)	N (R) (4)	N (I) (5)
2006	7	51	30	91
2007	6	24	0	97
2008	8	81	134	154
2009	34	619	656	738
2010	16	198	370	297
2011	1	3	3	2
2012	12	50	153	54

Notes: Column (1) is the year of observations; Col. (2) is the number of nights; Cols. (3), (4) and (5) are the number of data points in V, R and I bands respectively.

Table 2 The Magnitude Measurements of OJ 287 in the V Band

Date (UT) (1)	MJD (2)	Magnitude (3)	σ (4)
2012 Dec 24	56285.841	15.717	0.053
2012 Dec 24	56285.846	15.856	0.053
2012 Dec 24	56285.850	15.931	0.053
2012 Dec 24	56285.855	15.880	0.053
2012 Dec 21	56282.766	15.678	0.017
2012 Dec 21	56282.777	15.670	0.017
2012 Dec 21	56282.783	15.674	0.017
2012 Dec 20	56281.759	15.604	0.035

Notes: The full results are available in machine-readable form (*http://pan.baidu.com/s/1eSpbfLC*). The meaning of each column is the same as that in Table 2. As an illustration, the partial table content is given. Columns (1) and (2) are the date of observations and corresponding modified Julian day (MJD) respectively. Columns (3) and (4) are the magnitudes and corresponding errors respectively.

Table 3 The Magnitude Measurements of OJ 287 in the R Band

Date (UT) (1)	MJD (2)	Magnitude (3)	σ (4)
2012 Dec 24	56285.839	15.406	0.044
2012 Dec 24	56285.844	15.517	0.044
2012 Dec 24	56285.848	15.471	0.044
2012 Dec 24	56285.852	15.442	0.044
2012 Dec 21	56282.862	15.378	0.018
2012 Dec 21	56282.864	15.381	0.018
2012 Dec 21	56282.866	15.319	0.018
2012 Dec 21	56282.868	15.346	0.018
2012 Dec 21	56282.869	15.331	0.018

Notes: The full results are available in machine-readable form (*http://pan.baidu.com/s/1eSpbfLC*). The meaning of each column is the same as that in Table 2.

3.1.1 C-test

Jang & Miller (1997) first introduced the C-test, and then it was further developed by Romero et al. (1999). The C-test is a frequently employed method to measure whether a blazar is variable or not. The variability detection pa-

Table 4 The Magnitude Measurements of OJ 287 in the I Band

Date (UT) (1)	MJD (2)	Magnitude (3)	σ (4)
2012 Dec 24	56285.840	14.971	0.021
2012 Dec 24	56285.845	14.931	0.021
2012 Dec 24	56285.849	14.908	0.021
2012 Dec 24	56285.853	14.893	0.021
2012 Dec 21	56282.770	14.713	0.032
2012 Dec 21	56282.775	14.730	0.032
2012 Dec 21	56282.781	14.735	0.032
2012 Dec 21	56282.786	14.715	0.032
2012 Dec 20	56281.774	14.658	0.007
2012 Dec 20	56281.779	14.657	0.007

Notes: The full results are available in machine-readable form (*http://pan.baidu.com/s/1eSpbfLC*). The meaning of each column is the same as that in Table 2.

rameter C is defined as the average value of C_1 and C_2:

$$C_1 = \frac{\sigma(\mathrm{BL}-\mathrm{StarA})}{\sigma(\mathrm{StarA}-\mathrm{StarB})},$$
$$C_2 = \frac{\sigma(\mathrm{BL}-\mathrm{StarB})}{\sigma(\mathrm{StarA}-\mathrm{StarB})},$$

where (BL–StarA), (BL–StarB) and (StarA–StarB) are the differential instrumental magnitudes of the blazar and comparison StarA, the blazar and comparison StarB, and comparison StarA and StarB respectively. σ is the standard deviation of the differential instrumental magnitudes. If $C \geq 2.576$, the object will be reported as variable at a confidence level of 99 per cent. Despite the C-statistic having been widely used for differential photometry, de Diego (2010) pointed out that it has several problems.

3.1.2 F-test

In order to study stellar variability, the F-test was introduced by Howell et al. (1988). Afterwards, a lot of research efforts used this criterion to quantify optical variability of blazars (de Diego 2010; Hu et al. 2014; Agarwal & Gupta 2015). The F value is calculated from the average of F_1 and F_2:

$$F_1 = \frac{\mathrm{Var}(\mathrm{BL}-\mathrm{StarA})}{\mathrm{Var}(\mathrm{StarA}-\mathrm{StarB})},$$
$$F_2 = \frac{\mathrm{Var}(\mathrm{BL}-\mathrm{StarB})}{\mathrm{Var}(\mathrm{StarA}-\mathrm{StarB})},$$

where Var(BL–StarA), Var(BL–StarB) and Var(StarA–StarB) are the variances of differential instrumental magnitudes between blazar and StarA, blazar and StarB, and StarA and StarB, respectively. The F value is compared with the critical F-value, $F^{\alpha}_{\nu_{\rm bl},\nu_*}$, where $\nu_{\rm bl}$ and ν_* ($\nu = N-1$) stand for the number of degrees of freedom for the blazar and comparison star, respectively, and α is the significance level set as 0.01 (2.6σ). The critical values of the F-test can be given by the F-statistic. If the F value is larger than the critical value ($F^{\alpha}_{\nu_{\rm bl},\nu_*}$), the null hypothesis (no variability) is discarded.

3.1.3 ANOVA-test

Analysis of variance (ANOVA; de Diego 2010) is a powerful tool to detect microvariability. It does not depend on the error measurement, but derives the expected variance from subsamples of data. Considering different exposure times for our observations, this method is used only for light curves with more than 9 or 15 observations. For a given night, the data are divided into sub-groups. If the exposure time is from 50 to 150 s, each group has five observations. If the exposure time is from 150 to 300 s, each group has three observations (de Diego 2010; Xiong et al. 2016). If the measurements in the last group are less than 5 or 3 respectively, then it is merged with the previous group. The critical value of ANOVA can be obtained by $F^{\alpha}_{\nu_1,\nu_2}$ with the associated F-statistic, where $\nu_1 = k-1$ (k is the number of groups), $\nu_2 = N-k$ (N is the number of measurements) and α is the significance level.

3.1.4 Microvariability

If the data on a night pass all three tests, the blazar is regarded as a variable. If any one test is satisfied, the blazar is considered as a possible variable. The blazar is considered as non-variable if none of the criteria are satisfied. Based on our analysis, 16 nights show possible variability. As an example, some light curves for the possible variable nights are given in Figure 2. Table 5 lists the results on IDV. If we consider the square roots of the critical values for the F-test as the real critical value of the C-test (Villforth et al. 2010b; Goyal et al. 2013), there is one night detected with IDV (I band on 2009 April 15) which satisfies the three criteria of C-test, F-test and ANOVA. The magnitude changes are ΔI = 0.026 mag in 138 minutes from MJD = 54936.608 to MJD = 54936.704 corresponding to the variability amplitude Amp=2.87%. However, the light curve in the I band for 2009 April 15 is discontinuous, which appears as a large gap. Therefore, we still do not consider the night detection as reliable IDV.

When calculating the value of Amp, we only consider the nights with possible variability. Figure 3 shows

Table 5 Results of Intraday Observations of OJ 287

Date (UT) (1)	Band (2)	N (3)	C (4)	F (5)	$F_{\rm C}$ (99) (6)	$F_{\rm A}$ (7)	$F_{\rm A}$(99) (8)	V/N (9)	Time resolution (min) (10)	Time span (h) (11)	A (%) (12)
2006 Dec 01	V	18	0.87	0.70	3.24	2.23	6.36	N	2.50	1.16	-
2006 Dec 01	I	49	1.33	0.64	1.98	2.54	2.99	N	1.56	2.23	-
2007 Jan 24	I	42	1.18	1.59	2.10	6.24	3.23	PV	2.00	2.28	3.58
2007 Apr 15	I	19	0.29	0.30	3.13	1.01	5.29	N	2.20	0.93	-
2007 May 09	I	20	0.85	1.73	3.03	1.42	5.29	N	2.47	0.94	-
2008 Jan 10	R	20	0.69	0.52	3.03	1.85	5.29	N	2.50	0.83	-
2008 Jan 10	I	20	0.72	0.66	3.03	6.29	5.29	PV	2.00	1.59	2.52
2008 Jan 11	I	20	0.81	0.71	3.03	0.48	5.29	N	2.00	0.63	-
2008 Jan 11	R	14	1.60	4.55	3.91	1.29	7.21	N	2.50	0.55	-
2008 Jan 12	R	20	0.70	0.53	3.03	1.75	5.29	N	2.50	0.80	-
2008 Jan 12	I	20	0.72	0.57	3.03	0.18	5.29	N	2.00	0.63	-
2008 Apr 21	V	20	1.15	1.38	3.03	1.47	5.29	N	0.92	0.94	-
2008 Apr 21	R	20	1.31	1.72	3.03	18.79	5.29	PV	0.75	0.47	2.43
2008 Apr 21	I	20	1.07	1.14	3.03	5.04	5.29	N	0.41	0.90	-
2008 Apr 22	V	15	1.05	1.16	3.70	6.93	6.93	PV	0.91	0.77	2.54
2008 Apr 22	R	15	1.42	2.03	3.70	7.23	6.93	PV	0.75	0.42	2.17
2008 Apr 22	I	15	0.97	0.95	3.70	3.97	6.93	N	0.41	0.41	-
2008 Apr 23	V	20	0.98	1.05	3.03	2.66	5.29	N	0.92	0.69	-
2008 Apr 23	R	20	1.27	1.71	3.03	2.41	5.29	N	0.6	0.67	-
2008 Apr 23	I	20	0.86	0.74	3.03	1.62	5.29	N	0.41	0.66	-
2008 May 24	V	20	0.56	0.32	3.03	1.74	5.29	N	0.80	0.25	-
2008 May 24	I	20	0.81	0.65	3.03	3.83	5.29	N	1.30	0.40	-
2008 May 25	R	20	0.81	0.73	3.03	0.32	5.29	N	0.62	0.19	-
2008 May 25	I	19	0.66	0.45	3.13	0.09	6.23	N	0.79	0.33	-
2009 Jan 16	I	25	0.99	1.05	2.62	19.56	3.93	PV	4.32	2.38	3.31
2009 Jan 21	I	20	0.83	0.74	3.03	3.73	4.69	N	5.15	1.85	-
2009 Apr 13	V	17	0.83	0.77	3.37	0.23	6.51	N	4.80	0.87	-
2009 Apr 13	R	17	0.70	0.55	3.37	5.12	6.51	N	4.80	0.78	-
2009 Apr 13	I	18	0.86	0.74	3.24	0.52	6.36	N	4.80	0.79	-
2009 Apr 15	V	31	1.38	1.89	2.38	14.76	3.85	PV	2.00	2.91	2.45
2009 Apr 15	R	31	1.16	1.36	2.38	8.21	3.85	PV	2.00	2.90	2.27
2009 Apr 15	I	31	1.54	2.42	2.38	10.03	3.85	PV	2.00	2.91	2.87
2009 Apr 16	R	20	0.85	0.72	3.03	2.70	5.29	N	1.81	0.99	-
2009 Apr 16	I	15	0.79	0.66	3.70	1.42	6.93	N	1.81	0.98	-
2009 May 11	I	15	0.74	0.55	3.70	1.14	6.93	N	1.83	0.61	-
2009 Oct 24	V	33	0.63	0.55	2.32	2.22	3.78	N	1.55	0.83	-
2009 Oct 24	R	33	0.65	0.48	2.32	1.56	3.78	N	1.55	0.83	-
2009 Oct 24	I	33	0.81	0.75	2.32	0.39	3.78	N	1.55	0.83	-
2009 Oct 26	V	88	0.61	0.38	1.65	0.86	2.26	N	0.95	1.40	-
2009 Oct 26	R	88	0.76	0.67	1.65	2.92	2.26	PV	0.95	1.41	4.80
2009 Oct 26	I	88	0.71	0.60	1.65	2.51	2.26	PV	0.95	1.40	5.42
2009 Oct 27	V	26	0.81	0.66	2.60	0.17	4.37	N	1.53	0.73	-
2009 Oct 27	R	26	1.09	1.19	2.60	1.23	4.37	N	1.53	0.74	-
2009 Oct 27	I	26	1.36	1.86	2.60	1.39	4.37	N	1.53	0.72	-
2009 Oct 28	V	42	1.20	1.45	2.10	4.29	3.22	PV	1.53	1.05	6.52
2009 Oct 28	R	42	0.94	0.88	2.10	1.43	3.22	N	1.53	1.05	-
2009 Oct 28	I	42	0.74	0.56	2.10	1.02	3.22	N	1.53	1.05	-
2009 Oct 29	V	49	0.91	0.90	1.99	6.99	2.99	PV	1.54	1.24	3.69
2009 Oct 29	R	49	0.96	1.03	1.99	7.19	2.99	PV	1.54	1.24	3.92
2009 Oct 29	I	45	1.02	1.05	2.04	1.04	3.07	N	1.54	1.24	-
2009 Oct 30	V	61	1.19	1.42	1.84	15.87	2.63	PV	1.15	1.19	4.84
2009 Oct 30	R	13	1.26	1.60	4.16	3.11	7.56	N	1.55	1.25	-
2009 Oct 30	I	61	0.93	0.95	1.84	8.60	2.63	PV	1.15	1.26	8.27
2009 Nov 06	V	73	0.68	0.51	1.74	2.01	2.45	N	0.96	1.19	-
2009 Nov 06	R	73	0.68	0.48	1.74	2.13	2.45	N	0.96	1.19	-
2009 Nov 06	I	71	0.62	0.45	1.75	1.196	2.45	N	0.96	1.19	-
2009 Nov 10	V	19	0.88	0.82	3.03	3.11	5.42	N	0.30	0.09	-

Notes: Columns are as follows: (1) date of observation; (2) photometric band; (3) number of photometric images; (4) result of the C test; (5) average F value; (6) critical F value with a 99% confidence level; (7) value of ANOVA; (8) critical F value of ANOVA with a 99% confidence level; (9) variability status (PV: probable variable, N: non-variable); (10) and (11) time intervals and the time spans respectively; (12) variability amplitude.

Table 5 — *Continued.*

Date (UT) (1)	Band (2)	N (3)	C (4)	F (5)	$F_{\rm C}(99)$ (6)	$F_{\rm A}$ (7)	$F_{\rm A}$ (99) (8)	V/N (9)	Time resolution (min) (10)	Time span (h) (11)	A (%) (12)
2009 Nov 10	R	59	0.77	0.65	1.86	2.20	2.72	N	0.20	0.42	-
2009 Nov 10	I	30	0.71	0.57	2.42	1.49	3.89	N	0.20	0.10	-
2009 Nov 12	V	15	0.82	0.77	3.70	1.44	6.93	N	0.30	0.16	-
2009 Nov 12	R	15	0.72	0.56	3.70	0.30	6.93	N	0.20	0.11	-
2009 Dec 03	V	34	0.64	0.50	2.29	1.05	3.75	N	1.55	2.77	-
2009 Dec 03	R	35	0.63	0.46	2.26	2.86	3.53	N	1.55	2.77	-
2009 Dec 03	I	33	0.82	0.79	2.32	2.41	3.78	N	1.55	2.77	-
2009 Dec 14	V	69	0.90	0.87	1.77	3.77	2.52	PV	1.00	1.10	2.77
2009 Dec 14	R	69	0.86	0.77	1.77	1.64	2.52	N	1.00	1.11	-
2009 Dec 14	I	69	0.87	0.77	1.77	7.47	2.52	PV	1.00	1.10	1.90
2010 Jan 06	V	63	0.72	0.60	1.82	1.02	2.62	N	0.40	1.01	-
2010 Jan 06	R	75	0.76	0.60	1.73	1.51	2.39	N	0.20	1.07	-
2010 Jan 06	I	60	0.78	0.62	1.88	3.58	2.64	PV	0.20	0.84	1.34
2010 Jan 09	V	25	0.84	0.71	2.62	12.13	4.43	PV	1.80	1.74	2.02
2010 Jan 09	R	25	0.69	0.61	2.62	4.07	4.43	N	1.48	1.73	-
2010 Jan 09	I	125	0.67	0.52	1.52	3.15	1.98	PV	0.99	3.30	2.99
2010 Jan 16	R	153	0.37	0.14	1.46	3.41	1.87	PV	0.20	3.17	1.84
2010 Feb 16	V	20	1.02	1.12	3.03	8.6	5.29	PV	1.15	0.71	2.15
2010 Feb 16	R	20	0.58	0.36	3.03	0.20	5.29	N	0.80	0.65	-
2010 Mar 11	V	30	0.80	0.64	2.42	2.94	3.90	N	0.30	2.01	-
2010 Mar 11	R	33	0.66	0.43	2.32	6.68	3.78	PV	0.22	2.02	1.71
2010 Mar 11	I	30	0.78	0.62	2.42	3.62	3.89	N	0.22	2.01	-
2012 Dec 19	R	14	1.12	1.31	3.91	0.98	6.55	N	2.70	1.02	-
2012 Dec 20	R	55	1.01	1.03	1.89	2.06	2.49	N	2.70	3.62	-
2012 Dec 21	R	70	1.19	1.47	1.76	1.07	2.04	N	2.70	3.87	-

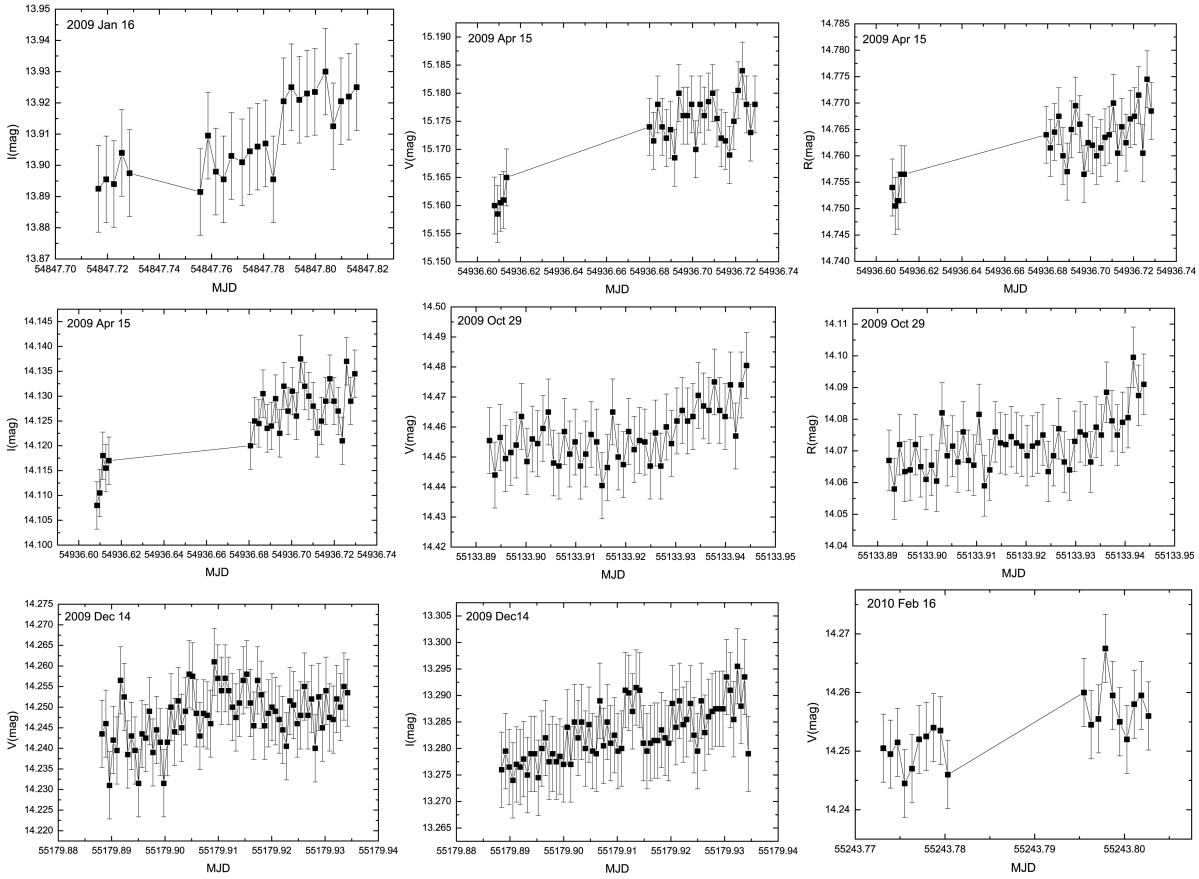

Fig. 2 The light curves with possible IDV for OJ 287.

the relative variability amplitude for all three bands, which ranges from 1% to 8%, with most of them falling in the range 2%–4%.

Fan et al. (2009) presented optical photometry results from 2002 to 2007 for the V, R and I bands. Their results showed that the object had strong activities. Intraday variations on timescales over 10 minutes to 2 hours were detected. The shortest timescale was 10 minutes with $\Delta R = 0.47$ mag and the largest magnitude variation $\Delta R = 0.75$ was over 32 minutes. Gupta et al. (2008) observed OJ 287 from 2006 to 2007 in the R band and found that the object did not show IDV on any of four nights. Gaur et al. (2012) reported that the object did not show genuine IDV on any of five nights between November 2009 and January 2010. For our results, no reliable IDV is detected, but possible variability is detected on 16 nights. Therefore during our monitoring epochs, the object had a low duty cycle of IDV. Based on previous IDV observational studies, the possibility of IDV detection is 80%–85% among observations with more than 6 hours each night. If the timescale is less than 6 hours, the possibility of IDV detection is 60%–65% (Gupta & Joshi 2005; Rani et al. 2011). For each night, the time span of our observations is less than 3 hours. Then to some extent, we cannot completely rule out the possibility that the low value of duty cycle may be caused by the time spans of our observations.

3.2 Time Lags

We employ the z-transformed discrete correlation function (ZDCF; Alexander 1997; Liu et al. 2008; Liao et al. 2014; Xiong et al. 2016) to search for time lags between different wavebands. The ZDCF can estimate the cross-correlation function in the case of nonuniformly sampled light curves. It is a binning type of method that is an improvement over the discrete correlation function (DCF; Edelson & Krolik 1988) technique. The result of ZDCF is more robust than that of DCF when applied to sparsely and unequally sampled light curves (Edelson et al. 1996; Giveon et al. 1999; Roy et al. 2000; Liu et al. 2008). The ZDCF has a notable feature for the data which are binned by equal population size rather than equal bin width $\Delta\tau$ as in the DCF. For a long-term timescale, we use the daily average magnitude to establish the time lags. For intraday and short timescales, we only use the data in the cyclic mode, and analyze the correlation between the V band magnitude and I band magnitude. We apply a Gaussian fit to find the highest points of ZDCF. The Gaussian profile peaks denote the time lags between correlated light curves (Wu et al. 2012; Xiong et al. 2016). The results are shown in Figure 4. There are no significant time lags, but strong correlations between any two bands for our light curves have been found (with peak correlation coefficients 0.829–0.990).

3.3 Spectral Behavior

Optical spectral behavior has been frequently investigated aiming to put physical constraints on blazar variability mechanisms. In order to study the behavior of spectral variations, we analyze the relationships between color indices and magnitudes for the intraday timescale and all time-series data sets. For the color index, Galactic extinction has been corrected with the value from NED, which is based on the result from Schlafly & Finkbeiner (2011). For our data, we concentrate on color index $V-I$ and V magnitude for intraday timescales because V and I bands have more photometric data points. We only analyze the quasi-simultaneous data with data points $N \geq 20$ for each night.

Figure 5 shows the results of the correlations between $V-I$ color index and V magnitude on intraday timescales. The results of linear regression analysis show that for OJ 287 the bluer-when-brighter trend is dominant on intraday timescales.

Combining SMARTS and the Steward Observatory data, we use the average magnitudes of every day in our observations to explore the relationship between color index $V-R$ and V magnitude from 2006 to 2017. For comparison star 10, the magnitudes used by SMARTS are 0.08 mag brighter in the R band and 0.05 mag fainter in the V band compared with those used by us. Relative to the magnitudes of comparison star 4 from SMARTS, the magnitudes of comparison star 4 from Steward Observatory are 0.058 mag brighter in the R band and 0.017 mag fainter in the V band (González-Pérez et al. 2001). In order to eliminate the uncertainty caused by different magnitudes of the same comparison stars for different telescopes, we use the SMARTS comparison star as a reference to correct ours and the Steward Observatory data.

Figure 6 shows the results of correlations between color index and magnitude for a long-term timescale. The analysis of Spearman rank correlation coefficient shows that there is a significant correlation between the color index $V-R$ and V-band magnitude ($r = 0.315$, $P = 1\times10^{-6}$), which indicates the bluer-when-brighter trend.

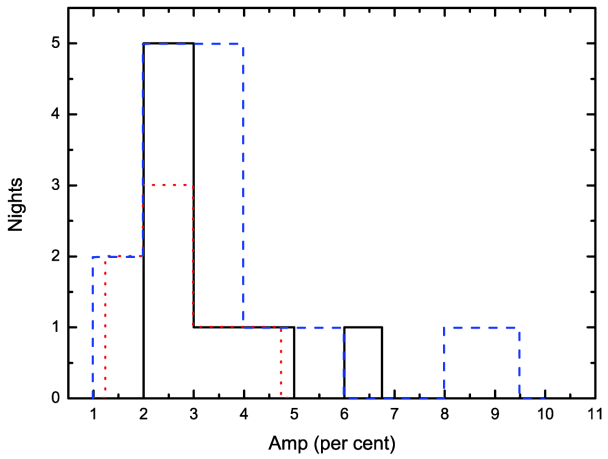

Fig. 3 The IDV amplitude distributions in I, R and V bands. The black solid line represents the V band, the red dotted line represents the R band and the blue dashed line represents the I band.

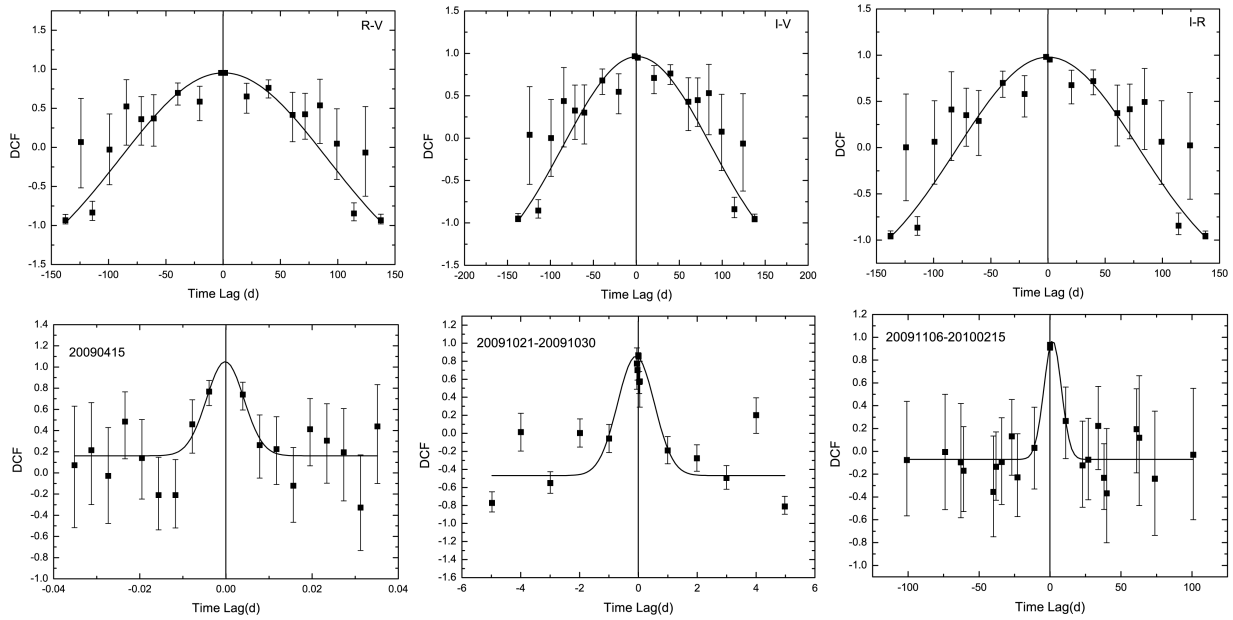

Fig. 4 The z-transformed DCF plots. The top panels show the results of ZDCF for daily average magnitude. The bottom panels present the results between V band magnitude and I band magnitude for intraday and short timescales. The curves show Gaussian fittings to the points. The vertical lines are the zero time lag.

Among our results, most of them show a strong bluer-when-brighter trend on intraday timescales. For the long-term timescale, it also shows a strong correlation between the color index and magnitude. So, the bluer-when-brighter chromatic trend is dominant for OJ 287. Sillanpaa et al. (1996) demonstrated that the object showed a constant optical color over a range of 2 mag in brightness. Through comparisons with outbursts of different periods, Hagen-Thorn et al. (1998) found that the spectral index depends on the peak level of the outburst, usually with a brighter outburst exhibiting flatter optical spectra. Vagnetti et al. (2003) found the bluer-when-brighter trend for the object. A bluer-when-brighter chromatism was also discovered by Wu et al. (2006). During the time between 2005–2009, the results of Villforth et al. (2010a) showed that OJ 287 had a bluer-when-brighter tendency. Dai et al. (2011) also reported a strong bluer-when-brighter chromatism from 2005 to 2009. The bluer-when-brighter behavior is most likely to support the shock-in-jet model (e.g. Gupta et al. 2008; Xiong et al. 2016). The shock-in-jet model supposes that as the shock is propagating down, the jet strikes a region

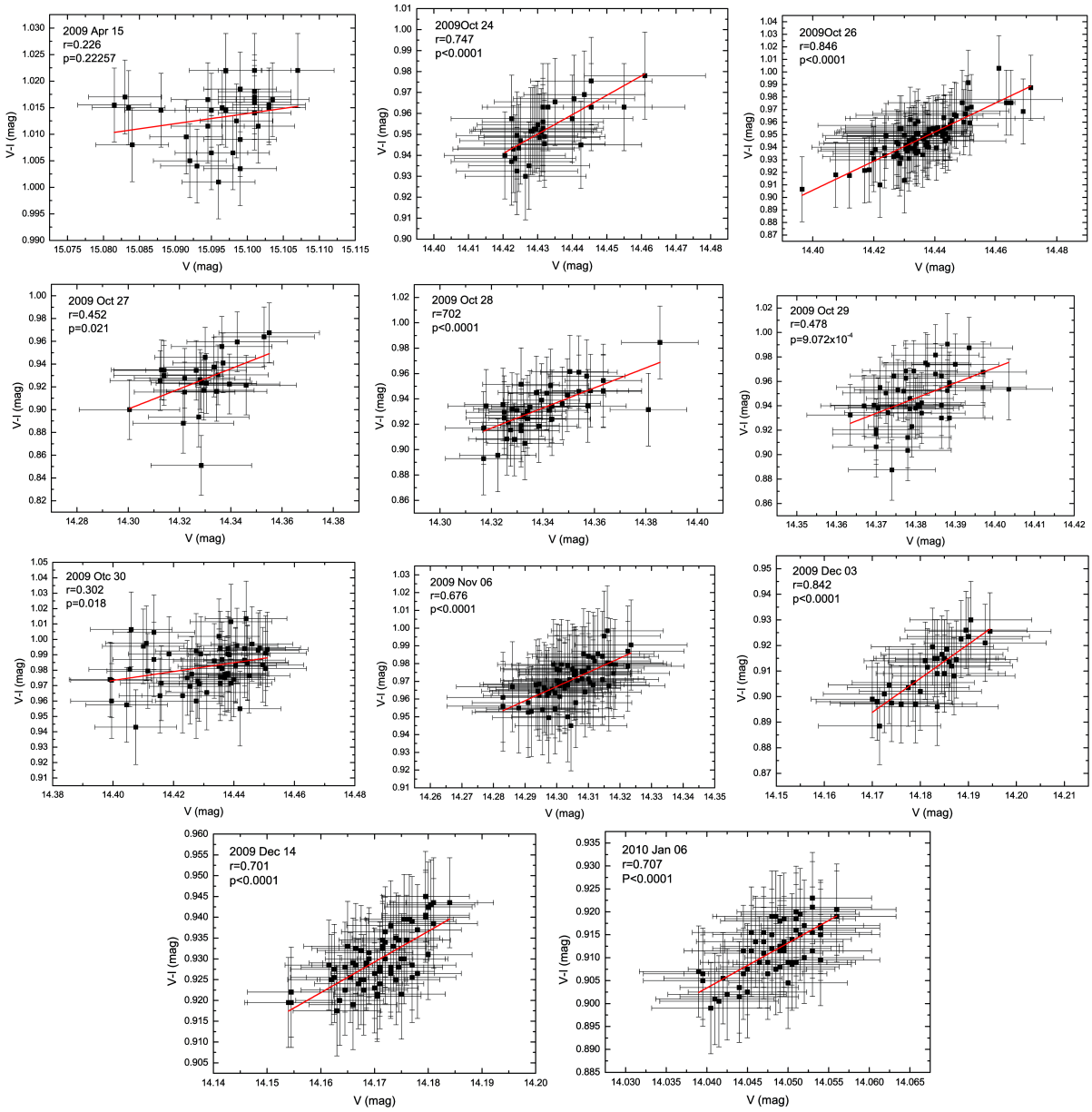

Fig. 5 The correlations between color index $V - I$ and V magnitude on an intraday timescale. The red solid lines are results of linear regression analysis. r is the linear regression coefficient of correlation and P is the chance probability.

with a high electron population, then radiation at different wavelengths is produced from different distances behind the shocks. High-energy photons from the synchrotron mechanism typically emerge sooner and closer to the shock front than lower frequency radiation, thus it can generate color variations (Agarwal & Gupta 2015). However, Bonning et al. (2012) found that the object showed redder-when-brighter changes but also a bluer-when-brighter trend. This phenomenon may be explained by the combination of two components that contribute to the overall emission in optical wavelengths, one variable with a blue component, and the other stable with a red component (Fiorucci et al. 2004; Gu et al. 2006). When the red component becomes dominant, the color behavior shows a redder-when-brighter trend. Otherwise, the color behavior shows a bluer-when-brighter trend.

3.4 Period Analysis

It is a notoriously arduous problem to search for periodicity in light curves. Especially for unevenly spaced pho-

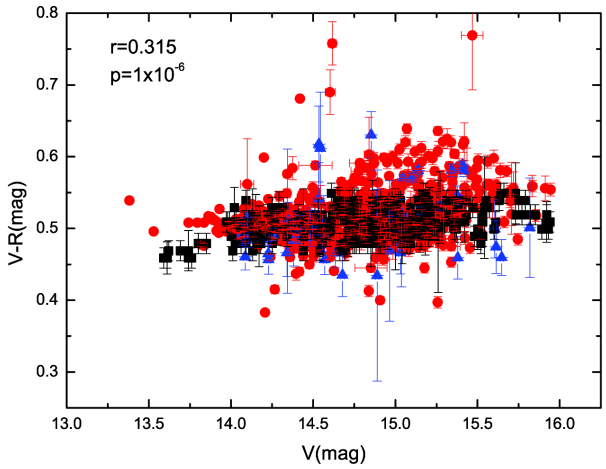

Fig. 6 The correlation between color index and magnitude for long-term timescale. The red circles are plotted from SMARTS data, the black squares represent Steward Observatory data and the blue triangles represent our data.

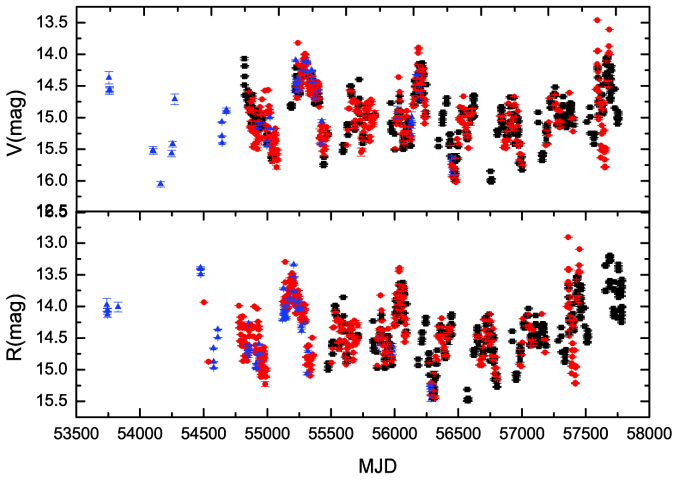

Fig. 7 The light curves from 2006 to 2017 in the V and R bands obtained from SMARTS (*red circles*), Steward Observatory (*black squares*) and our monitoring data (*blue triangles*).

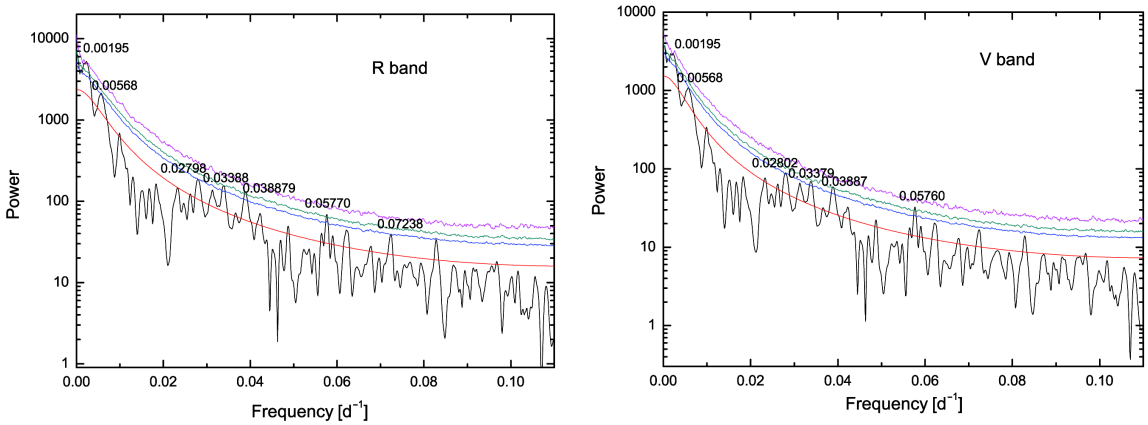

Fig. 8 The results of period analyses. The black line shows bias-corrected power spectra. Curves starting from the bottom are the theoretical red-noise spectrum, and 90%, 95% and 99% significance levels derived from the Monte Carlo technique, respectively. At 90% significance levels, the possible periods of V band are 513, 176, 37, 30, 26 and 17 d in the light curves. The possible periods of R band are 512, 176, 37, 30, 26, 17 and 14 d.

tometric data, the light curves are affected by frequency dependent red noise (Sandrinelli et al. 2016; Li et al. 2016). Combining our data with SMARTS and Steward Observatory monitoring data, we search the periodic signals of OJ 287 from 2006 to 2017. The light curves from 2006 to 2017 are shown in Figure 7. The magnitudes are firstly converted into fluxes (in mJy) using $F_R = 3080 \times 10^{-0.4*R} \times 10^3$ and $F_V = 3640 \times 10^{-0.4*V} \times 10^3$ for R and V bands respectively (Mead et al. 1990; Xiong et al. 2016). We employ a Fortran 90 program (REDFIT) to estimate the red noise through a first-order autoregressive (AR1) process (Schulz & Mudelsee 2002). The program can be used to test whether the peaks in the spectrum within a time series are significant against the red-noise background from an AR1 process, then it can remove the bias of this Fourier transform from unevenly spaced data by correcting the effect of correlation between Lomb-Scargle Fourier components. In addition, the Monte Carlo technique is used to assess the statistical significance of a spectral peak. The analyzed results of two bands are shown in Figure 8. At a 90% significance level, the possible periods of V-band are 513, 176, 37, 30, 26 and 17 d in the light curves. The possible periods of R-band are 512, 176, 37, 30, 26, 17 and 14 d. Both bands show almost the same periods.

Pihajoki et al. (2013) studied short-term variability for the object. They found a $\sim$50 d periodic component, presumably related to the half-period of the innermost stable circular orbit of the primary black hole. In their analysis, long periods of $\sim$500 d and $\sim$150 d were found. However, they did not consider the two periods partly due to effects of data sampling. Wu et al. (2006) presented a possible period of 40 d using both visual inspection and structure function analyses in three BATC wave bands during the first half year of 2005. By re-analyzing the optical data from the OJ-94 project, Wu et al. (2006) also confirmed another period of 40 d. Through studying the rotation of the position angle of the optical polarization, Efimov et al. (2002) detected an apparent period of 36.56 d. Combining the data from SMARTS and Steward Observatory, we also found the period of $\sim$40 d. Our new results support previous findings. Furthermore, our results show other possible periods: 512, 176, 30, 26, 17 and 14 d. For our sample, after checking the details of data sampling, we do not find that the periods derived here are related with the data sampling. For these periods, some possible interpretations include the orbit of a perturbing object, a precession in the jet, a helical structure of the magnetic field at the base of the jet, or the orbital motion of the accretion disk close to the central primary black hole (Efimov et al. 2002; Wu et al. 2006; Xiong et al. 2017).

4 SUMMARY

We present our photometric results from optical multicolor monitoring of the BL Lac object OJ 287 from January 2006 to December 2012. Our data include 84 nights and 3805 different CCD images. A relatively active state in OJ 287 has been found over all monitoring epochs, among which variations of average magnitude in $V/R/I$ bands were measured with $\Delta V = 1.956$ mag, $\Delta R = 2.067$ mag and $\Delta I = 2.115$ mag, respectively. No reliable IDV is detected, but possible variability is detected on 16 nights. Their variability amplitudes are from 1% to 8%, with the majority of them in the range of 2%–4%. From the ZDCF, there are no significant time lags, but there are powerful correlations between any two bands for our light curves. A bluer-when-brighter trend has been found for the intraday timescale, which can be explained by the shock-in-jet model. Combining with V band and R band data obtained from SMARTS and Steward Observatory, there is a bluer-when-brighter trend between color index $V - R$ and V magnitude for a long-term timescale. Some possible periods of 513, 176, 36, 30, 26, 17 and 14 d are found in all time-series data sets. The possible explanations are complicated, which may include the orbit of a perturbing object, a precession in the jet, a helical structure of the magnetic field at the base of the jet or orbital motion of the accretion disk close to the central primary black hole.

Acknowledgements We sincerely thank the referee for valuable comments and suggestions. We thank Shaokun Li, Liang Chen, Nenghui Liao and Jin Zhang for observations. We acknowledge support from the staff of the Lijiang 2.4 m and Kunming 1 m telescopes. Funding for the telescopes has been provided by CAS and the People's Government of Yunnan Province. This paper has made use of up-to-date SMARTS optical/near-infrared light curves that are available at *www.astro.yale.edu/smarts/glast/home.php*. Data from the Steward Observatory spectropolarimetric monitoring project were used. This program is supported by Fermi Guest Investigator grants NNX08AW56G, NNX09AU10G, NNX12AO93G and NNX15AU81G. This research is supported by the Strategic Priority Research Program of the Chinese Academy of Sciences

- The Emergence of Cosmological Structures (grant No. XDB09000000), the Key Research Program of the Chinese Academy of Sciences (grant No. KJZD-EW-M06), and the NSFC through NSFC-11133006 and 11361140347. DRX acknowledges support from Chinese Western Young Scholars Program and Light of West China Program provided by CAS.

References

Agarwal, A., & Gupta, A. C. 2015, MNRAS, 450, 541
Alexander, T. 1997, in Astrophysics and Space Science Library, 218, Astronomical Time Series, eds. D. Maoz, A. Sternberg, & E. M. Leibowitz, 163
Bonning, E., Urry, C. M., Bailyn, C., et al. 2012, ApJ, 756, 13
Böttcher, M. 2007, Ap&SS, 309, 95
Carini, M. T., Miller, H. R., Noble, J. C., & Goodrich, B. D. 1992, AJ, 104, 15
Dai, B.-z., Zeng, W., Jiang, Z.-j., et al. 2015, ApJS, 218, 18
Dai, Y., Wu, J., Zhu, Z.-H., Zhou, X., & Ma, J. 2011, AJ, 141, 65
de Diego, J. A. 2010, AJ, 139, 1269
Edelson, R. A., & Krolik, J. H. 1988, ApJ, 333, 646
Edelson, R. A., Alexander, T., Crenshaw, D. M., et al. 1996, ApJ, 470, 364
Efimov, Y. S., Shakhovskoy, N. M., Takalo, L. O., & Sillanpää, A. 2002, A&A, 381, 408
Fan, J. H., Zhang, Y. W., Qian, B. C., et al. 2009, ApJS, 181, 466
Fiorucci, M., Ciprini, S., & Tosti, G. 2004, A&A, 419, 25
Fiorucci, M., & Tosti, G. 1996, A&AS, 116, 403
Gaur, H., Gupta, A. C., Strigachev, A., et al. 2012, MNRAS, 425, 3002
Giveon, U., Maoz, D., Kaspi, S., Netzer, H., & Smith, P. S. 1999, MNRAS, 306, 637
González-Pérez, J. N., Kidger, M. R., & Martín-Luis, F. 2001, AJ, 122, 2055
Goyal, A., Gopal-Krishna, Paul J., W., Stalin, C. S., & Sagar, R. 2013, MNRAS, 435, 1300
Gu, M. F., Lee, C.-U., Pak, S., Yim, H. S., & Fletcher, A. B. 2006, A&A, 450, 39
Gupta, A. C., & Joshi, U. C. 2005, A&A, 440, 855
Gupta, A. C., Fan, J. H., Bai, J. M., & Wagner, S. J. 2008, AJ, 135, 1384
Hagen-Thorn, V. A., Marchenko, S. G., Takalo, L. O., et al. 1998, A&AS, 133, 353
Heidt, J., & Wagner, S. J. 1996, A&A, 305, 42
Howell, S. B., Warnock, III, A., & Mitchell, K. J. 1988, AJ, 95, 247
Hu, S. M., Chen, X., Guo, D. F., Jiang, Y. G., & Li, K. 2014, MNRAS, 443, 2940
Jang, M., & Miller, H. R. 1997, AJ, 114, 565
Li, H. Z., Jiang, Y. G., Guo, D. F., Chen, X., & Yi, T. F. 2016, PASP, 128, 074101
Liao, N. H., Bai, J. M., Liu, H. T., et al. 2014, ApJ, 783, 83
Liu, H. T., Bai, J. M., Zhao, X. H., & Ma, L. 2008, ApJ, 677, 884
Mead, A. R. G., Ballard, K. R., Brand, P. W. J. L., et al. 1990, A&AS, 83, 183
Pihajoki, P., Valtonen, M., & Ciprini, S. 2013, MNRAS, 434, 3122
Qian, B., & Tao, J. 2003, PASP, 115, 490
Rani, B., Gupta, A. C., Joshi, U. C., Ganesh, S., & Wiita, P. J. 2011, MNRAS, 413, 2157
Romero, G. E., Cellone, S. A., & Combi, J. A. 1999, A&AS, 135, 477
Roy, M., Papadakis, I. E., Ramos-Colón, E., et al. 2000, ApJ, 545, 758
Sandrinelli, A., Covino, S., Dotti, M., & Treves, A. 2016, AJ, 151, 54
Schlafly, E. F., & Finkbeiner, D. P. 2011, ApJ, 737, 103
Schulz, M., & Mudelsee, M. 2002, Computers and Geosciences, 28, 421
Sillanpaa, A., Haarala, S., Valtonen, M. J., Sundelius, B., & Byrd, G. G. 1988, ApJ, 325, 628
Sillanpaa, A., Takalo, L. O., Pursimo, T., et al. 1996, A&A, 305, L17
Smith, P. S., Montiel, E., Rightley, S., et al. 2009, arXiv:0912.3621
Takalo, L. O., & Sillanpaa, A. 1989, A&A, 218, 45
Vagnetti, F., Trevese, D., & Nesci, R. 2003, ApJ, 590, 123
Valtonen, M. J., Zola, S., Ciprini, S., et al. 2016, ApJ, 819, L37
Villforth, C., Nilsson, K., Heidt, J., et al. 2010a, MNRAS, 402, 2087
Villforth, C., Koekemoer, A. M., & Grogin, N. A. 2010b, ApJ, 723, 737
Wu, J., Zhou, X., Wu, X.-B., et al. 2006, AJ, 132, 1256
Wu, J., Böttcher, M., Zhou, X., et al. 2012, AJ, 143, 108
Xiong, D., Zhang, H., Zhang, X., et al. 2016, ApJS, 222, 24
Xiong, D., Bai, J., Zhang, H., et al. 2017, ApJS, 229, 21